PDF-analysis of local structure in disordered materials

Henry E. Fischer

Institut Laue-Langevin, Grenoble

Hercules Lecture
Friday 17 March 2023

Fundamental Concepts concerning Structure and Diffraction

Structure depends on time and length scales

An amorphous material has short-range order, but no long-range order, implying a small *structural correlation length* $\zeta_{\rm str}$.

Even in a “perfect crystal” with long-range *average* order, the atoms are moving thermally, such that the “structure” depends on both time and space. The atomic displacements (*e.g.* for a phonon) are thus characterised not only by a $\zeta_{\rm str}$, but also by a *structural correlation time* $\tau_{\rm str}$ aka lifetime or relaxation time.

A fluid (liquid, gas) can have a very short $\tau_{\rm str} \lesssim 1$ ps.

The structure of a system/material must therefore be defined with respect to given length and time scales, and also specify whether any averaging over time, space or ensembles is considered.

A structural measurement probes the structure of a system over a certain range in space and with a certain time resolution, and scattering methods along with their analyses may also involve statistical averaging over time, space, or ensembles.

Schematic of a diffraction measurement (mono-λ)

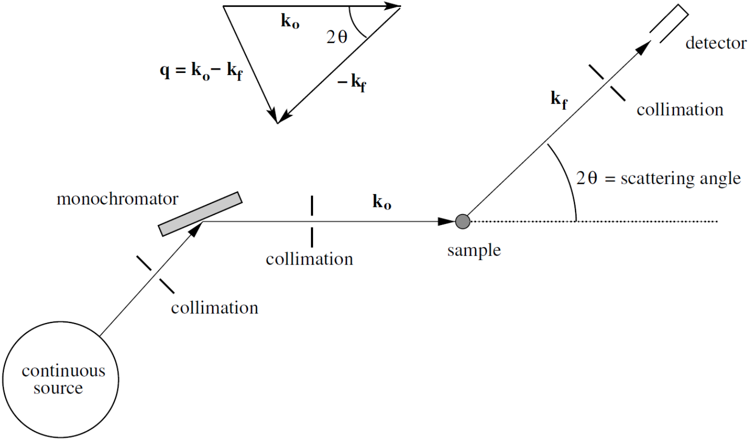

A detector counts *all* neutrons of incident wavevector $\mathbf{k}_\mathrm{o}$ and kinetic energy E_o that are scattered by a sample through a scattering angle 2θ with wavevector transfer $\mathbf{q} = \mathbf{k}_\mathrm{o} - \mathbf{k}_\mathrm{f}$, *regardless of energy loss* $\hbar\omega = E_\mathrm{o} - E_\mathrm{f}$, *which in fact defines a diffraction measurement*.

Schematic of a diffraction measurement (mono-λ)

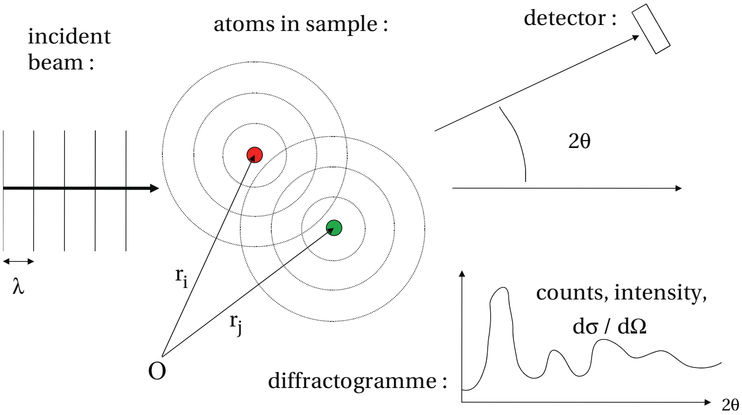

The spherical waves of probabilistic scattering amplitude from all the atoms in a given neutron's coherence volume ($\phi \sim 100$ Å) interfere with each other at the detector, producing a diffraction pattern as a function of the scattering angle 2θ or the scalar $q = (4\pi/\lambda)\,\sin(\theta)$.

Coherence volume = spatial range of measurement

Considering a neutron as a Gaussian wavepacket, its spatial localisation δx along x in the sample is limited by the information content $\hbar/2$ and coupled via the Uncertainty Principle $\delta x \cdot \delta p_x = \hbar/2$ to the constraints on its wavefunction $\delta k_x = \delta p_x/\hbar$ imposed by the energy-selective and collimating optical elements of the diffractometer **both upstream and downstream of the sample**.

This positional uncertainty δx is effectively the coherence length ξ_x of the neutron's wavepacket along x, and likewise for y and z.

The better the final q-space resolution of the diffraction pattern, the less information remains for localising the neutron in the sample, and thus *the statistical contribution of the neutron to the diffraction pattern is representative of the material's structure over a greater volume of positional uncertainty, namely the* coherence volume $V_{\text{coh}} = \xi_x \xi_y \xi_z$, which can be thought of as a modulation envelope or "visibility range" that delimits the neutron's wavefunction $\Psi(\mathbf{r}, t)$. (Feynman: $\sum_{\text{paths}}$).

The associated FWHM coherence length ξ_q along **q** in the diffraction plane is simply $\xi_q = 4\ln(4)/\Delta q = 5.55/\Delta q$, where Δq is the FWHM q-space resolution of the diffraction pattern.

Coherence volume of a neutron wavepacket

$\Psi(\mathbf{r},t)$ = probability amplitude for the propagating neutron's presence

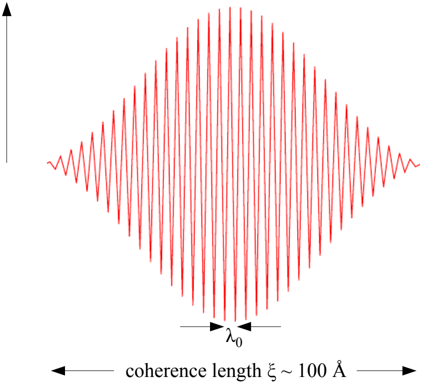

λ_0

coherence length $\xi \sim 100$ Å

$|\Psi(\mathbf{r},t)|^2$ = probability of finding the neutron at position **r** at time t

Propagation direction:

$\longrightarrow$ $\mathbf{k_0}$ = wavevector

$k_0 = |\mathbf{k_0}| = 2\pi/\lambda_0$

$E_0 = \hbar\omega_0 = \hbar^2 k_0^2 / 2m$

spread in wavelength:

$\Delta\lambda/\lambda = \Delta k/k \sim 1\ \%$

A Gaussian wavepacket of incident $\hbar\omega_0$ and central wavevector $\mathbf{k_0}$ is localized in position within *e.g.* $\xi_x = \delta x = \hbar/2\delta p_x = 1/2\delta k_x$ and propagates with group velocity $v_g = \mathrm{d}\omega/\mathrm{d}k$. The scattered neutron has “seen” only the 100,000 or so atoms that “felt” its wavefunction $\Psi(\mathbf{r},t)$ within the coherence volume $V_{\mathrm{coh}} \sim \xi_x\xi_y\xi_z$.

Coherence time = time resolution of measurement

The *temporal* localisation δt of a neutron wavepacket in the sample is also limited by information content of $\hbar/2$ and coupled via $\delta t \cdot \delta E = \hbar/2$ to the constraints on its wavefunction $\delta\omega = \delta E/\hbar$ imposed by energy selective optical elements **both upstream and downstream of the sample**, *e.g.* monochromators, choppers, velocity selectors, analysers.

This temporal uncertainty δt is effectively the coherence time $\tau_{\rm coh}$ of the neutron's wavepacket in the sample upon scattering, and represents the "instantaneousness" or the *duration* of the scattering "event" ($\neq$ Einst.).

The better the final energy resolution δE of the diffraction pattern, or of an extracted part of it such as integrated Bragg peak intensities, the less information remains for the timing of the scattering "event", and thus *the statistical contribution of the neutron to the diffraction pattern is representative of the material's structure (within $V_{\rm coh}$) as averaged over a greater duration of time, namely the coherence time $\tau_{\rm coh}$*.

Since in general a diffraction measurement involves no energy analysis of the scattered neutrons, the final energy resolution $\delta E \sim E_0$, leading to a very small $\tau_{\rm coh}$ and thus to nearly instantaneous time resolution, *when all of the diffracted intensity is made use of in the data analysis*.

Interference from 2 diffracting atoms

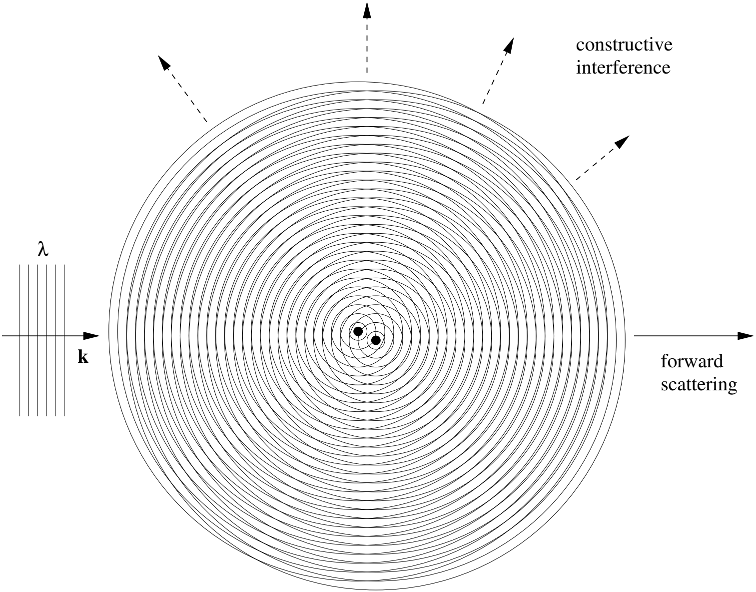

Interference from an ordered line of 3 atoms

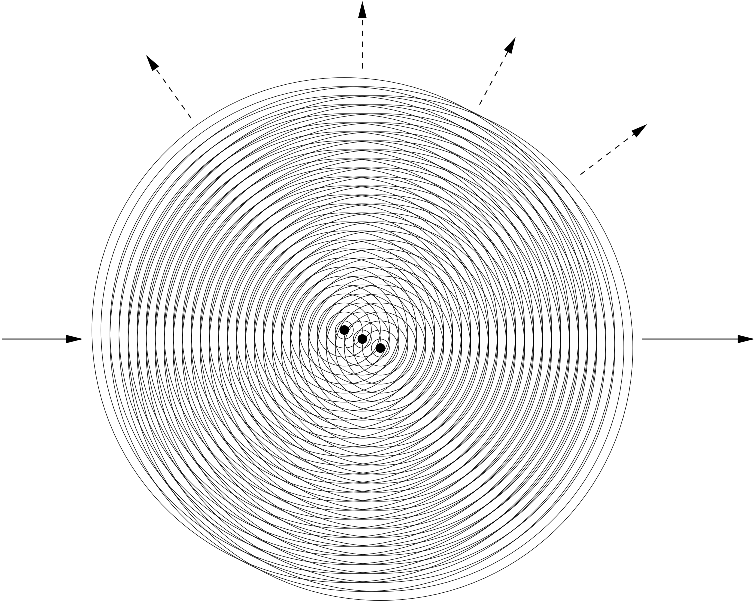

Interference from an ordered array of 9 atoms

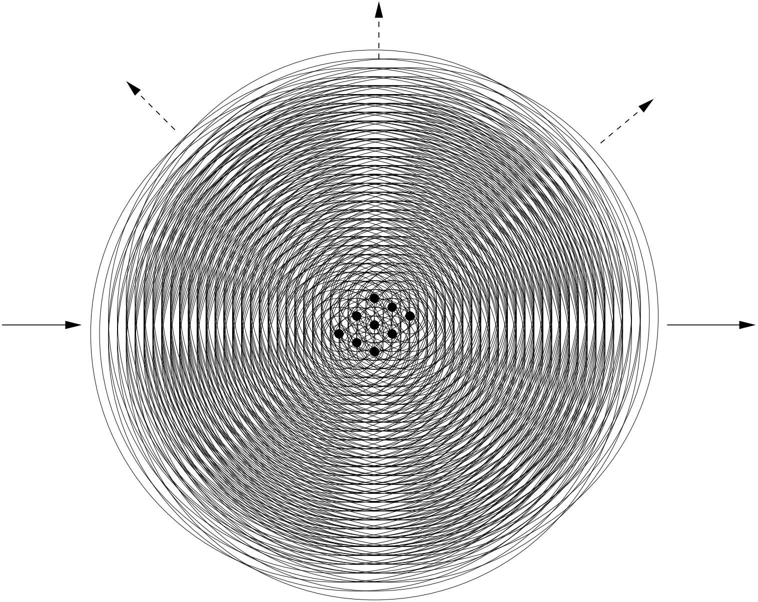

Diffraction intensity as reflected from Bragg planes

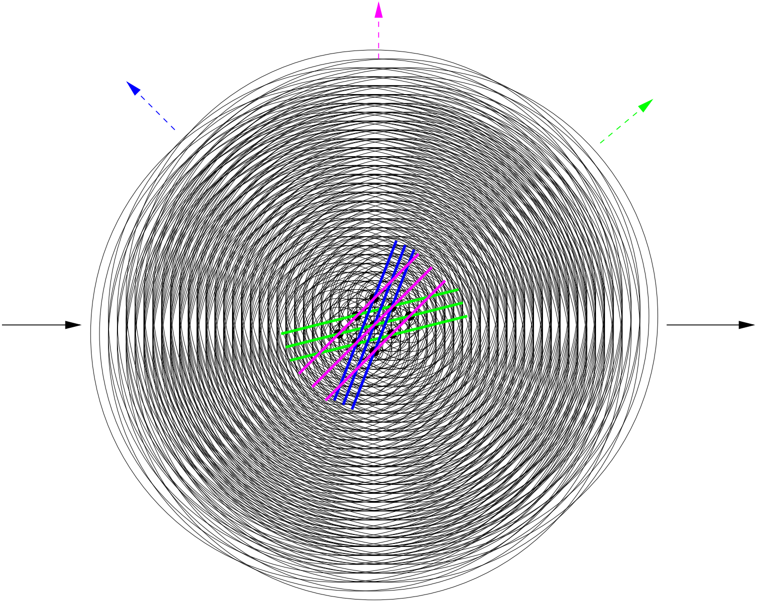

Diffraction intensity from an ensemble of atoms

Constructive interference at the detector results when the path lengths followed by a neutron wave, as scattered by two different atoms, differ by a multiple of λ. This also holds for “reflection” from parallel atomic planes of period *d* as shown by Bragg’s law: $n\lambda = 2d\,\sin(\theta)$.

A pathlength difference of $n\cdot\lambda$ means a phase difference of $n\cdot 2\pi$. So, we can sum up all the scattered amplitudes b_i and phases from all the diffracting atoms (*i.e.* within V_{coh}) at positions $\mathbf{r}_i$ and write the total scattered amplitude propagating along $\mathbf{k}_{\mathrm{f}}$ towards the detector:

$$A_{\mathrm{diff}}(\mathbf{q}) = \sum_i^N b_i\, e^{i\mathbf{q}\cdot\mathbf{r}_i} \qquad b_i = \text{"scattering length"}$$

where $\mathbf{q} = \mathbf{k}_{\mathrm{o}} - \mathbf{k}_{\mathrm{f}}$ as before, and for now $|\mathbf{k}_{\mathrm{f}}| = |\mathbf{k}_0| = k$. The diffracted intensity or counting rate recorded by the detector is then:

$$I(\mathbf{q}) \propto |A_{\mathrm{diff}}(\mathbf{q})|^2 = \left|\sum_i^N b_i\, e^{i\mathbf{q}\cdot\mathbf{r}_i}\right|^2 = \sum_{i,j}^N b_i b_j^*\, e^{i\mathbf{q}\cdot\mathbf{r}_{ij}} \;,$$

where $\mathbf{r}_{ij} = \mathbf{r}_i - \mathbf{r}_j$ is the relative position of atom *i* with respect to atom *j*, and * denotes the complex conjugate. Since phase information is lost in an intensity measurement, we cannot directly deduce the absolute positions of the atoms from the diffraction pattern.

Diffuse intensity from a disordered array of 9 atoms

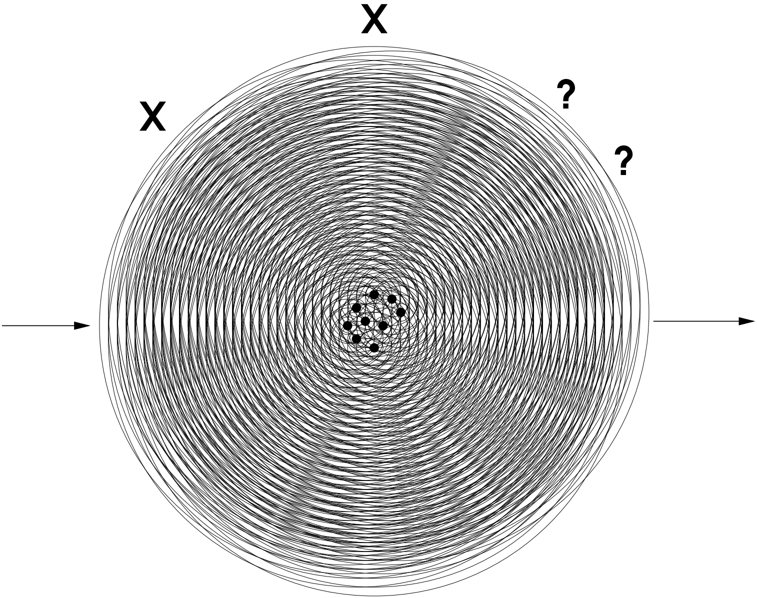

How disordered is “disordered” ?

A completely “disordered” system has no positional nor orientational correlations between scattering centers (atoms, molecules, magnetic spins), leading to an isotropic diffraction pattern $I(q)$. However, zero *positional* correlation can be hard to achieve, even in the case of the minimal constraints of the Percus-Yevick hard-sphere fluid potential:

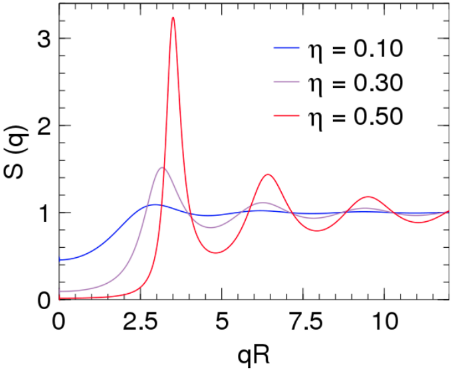

$S(q) \propto I(q)$

R = hard-sphere radius

η = packing fraction

(courtesy of Wikipedia)

Even at low densities η, diffraction detects correlations, *i.e.* some structural “order”, revealed by the shape of the diffuse scattering.

Substitution of A vs B atoms on a square lattice

Disordered Structures

Partial cross section of 200x200 unit cell model crystals
Composition 75% A 25% B

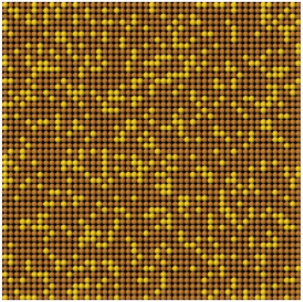

Random position of A B atoms

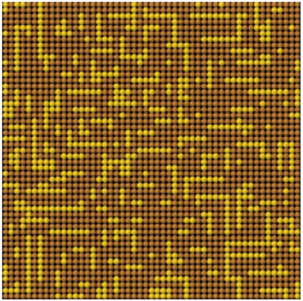

Non-random position of A B atoms

Properties of the two crystals will differ

(courtesy of R. Neder).

Bragg: sees an average atom at each lattice site

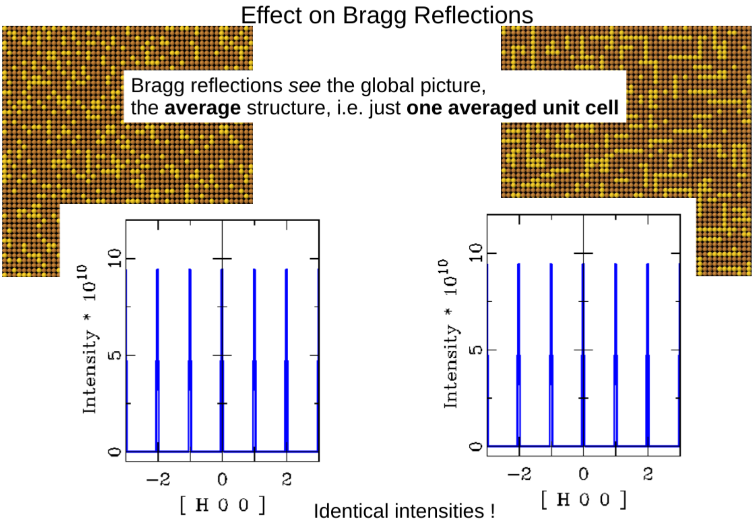

Bragg reflections *see* the global picture,
the **average** structure, i.e. just **one averaged unit cell**

Identical intensities !

(courtesy of R. Neder).

Diffuse: sees all correlations between A & B atoms

Diffuse scattering to the rescue ...

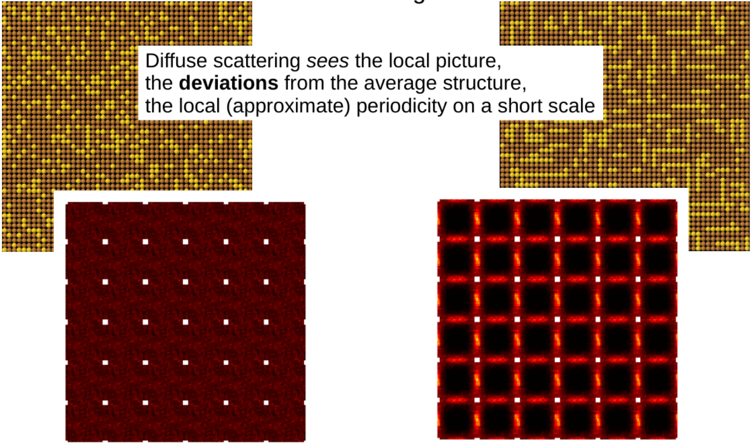

Diffuse scattering *sees* the local picture,
the **deviations** from the average structure,
the local (approximate) periodicity on a short scale

Continuous unstructured scattering

Modulated diffuse scattering

(courtesy of R. Neder).

Magnetic diffuse scattering & spin-spin correlations

Zero orientational correlations between spins are achieved in a purely paramagnetic state, but partial orientational disorder can look a lot like orientational order at first glance in *r*-space, but not in *q*-space where diffuse scattering is very sensitive to deviations from perfect (dis)order:

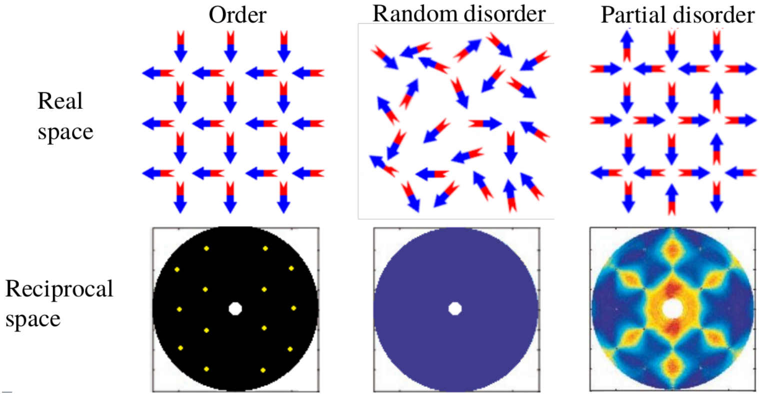

(courtesy of T. Northam).

Total scattering, $S(\mathbf{q},\omega)$, and time scales

A diffraction pattern integrates over all sample-neutron *E*-transfers:

$$\left.\frac{d\sigma}{d\Omega}(\mathbf{q})\right|_{\mathrm{meas}} = \int_{-\infty}^{E_o} d(\hbar\omega)\,\frac{\sigma}{4\pi}\,\frac{k_f}{k_o}\,N\,S(\mathbf{q},\omega)\ ,$$

whence $\delta E \sim E_o$ and $\tau_{coh} = \delta t \sim \hbar/(2\delta E) \sim 1$ fs for $\lambda = 0.5$ Å, thus representing a quasi-instantaneous “snapshot” of the sample’s local structure, as ensemble-averaged over coherence volumes.

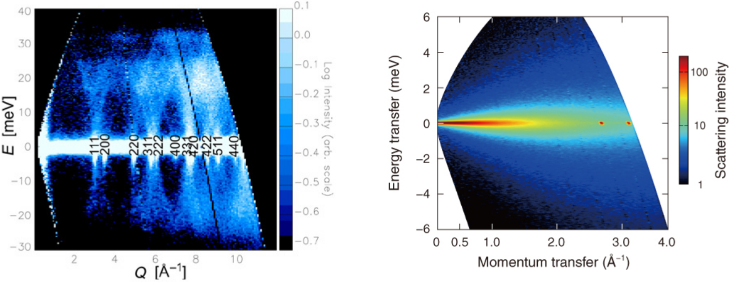

Rietveld refinement of *elastic* Bragg peaks disregards the inelastic scattering containing information about *dynamic* atomic correlations (*e.g.* phonons) and represents the sample’s time-averaged structure.

Total scattering, diffuse intensity, and length scales

In addition, the refinement of diffraction intensity only at Bragg-peak positions neglects the inter-peak diffuse intensity, which when elastic represents time-averaged or *static* local atomic correlations.

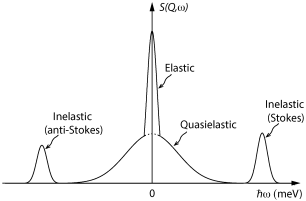

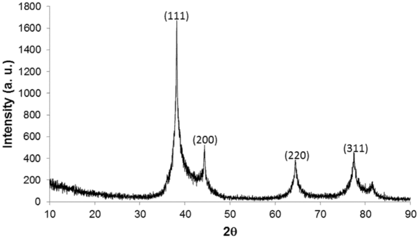

By neglecting the diffuse intensity between (and "under") Bragg peaks, Rietveld refinement additionally performs a spatial average over each neutron coherence volume, resulting in a time+space averaged picture of the sample's structure, which is very useful for crystallography.

By retaining all the original information in the differential cross-section $(d\sigma/d\Omega)(\mathbf{q})$ measured via diffraction, total-scattering represents an ensemble average of quasi-instantaneous snapshots of local structures (*i.e.* within each neutron coherence volume) throughout the sample.

The static approximation for total scattering

When the incident energy E_o exceeds the maximum possible energy transfer $\hbar\omega_{\text{max}}$ between the scattered neutron and the excitations in the sample, and for $\varepsilon(E_f) = 1$, it is perfectly valid to use the *static approximation* to derive the *differential scattering cross-section* for diffraction as a function of $\mathbf{q}$ only (note that $q \ll k_o \Rightarrow k_f/k_o \sim 1$):

$$\frac{d\sigma}{d\Omega}(\mathbf{q}) = \int_{-\infty}^{\omega\to\infty} d\omega \, N\frac{\sigma_s}{4\pi}\, S(\mathbf{q},\omega) \overset{\text{s.a.}}{=} \overline{\left\langle \left| \sum_{i}^{N} b_i\, e^{i\mathbf{q}\cdot\mathbf{r}_i} \right|^2 \right\rangle} = \left\langle \sum_{i,j}^{N} \overline{b_i b_j^*}\, e^{i\mathbf{q}\cdot\mathbf{r}_{ij}} \right\rangle ,$$

where b_i is the scattering length of the i^{th} atom at position $\mathbf{r}_i$, and $\mathbf{r}_{ij} = \mathbf{r}_i - \mathbf{r}_j$. The $<>$ represent a thermal average and the horizontal bars an ensemble average over the different possible coherence volumes within the sample, each having a particular assignment of scattering lengths in the case of neutron diffraction.

$\Rightarrow (d\sigma/d\Omega)(\mathbf{q})$ measures an *ensemble average* of quasi-instantaneous snapshots of local structures (*i.e.* within the neutron coherence volume) throughout the sample volume over the duration of the experiment.

The extracted elastic integrated Bragg peak intensities provide however only a time+space averaged picture of the structure.

Atomic PDF-analysis

Case of a monoatomic sample (only one Z)

In neutron scattering, a monoatomic sample can have a distribution of scattering lengths b_i, but there is no correlation between b_i and the structural environment of $\mathbf{r}_i$. The ensemble average over coherence volumes then leads to an expression (units of barns/str/atom) involving a **q**-dependent coherent term and an isotropic incoherent term:

$$\frac{1}{N}\left[\frac{d\sigma}{d\Omega}(\mathbf{q})\right] = \overline{b}^2 S(\mathbf{q}) + \left(\overline{b^2} - \overline{b}^2\right)$$

where the sample's average scattering length $\overline{b} = b_{\mathrm{coh}}$, the scattering cross-section $\sigma_s = 4\pi\overline{b^2}$, and $\left(\overline{b^2} - \overline{b}^2\right) = var(b)$ is simply the variance of scattering lengths throughout the sample. ⇒ Incoherent scattering is merely a result of ensemble-averaging over the coherence volumes of the different scattered neutrons. The alternative expression:

$$\frac{1}{N}\left[\frac{d\sigma}{d\Omega}(\mathbf{q})\right] = \overline{b}^2\left[S(\mathbf{q}) - 1\right] + \overline{b^2}$$

comprises a “distinct” term (interference between different atoms) and a “self” term (self-interference from individual atoms).

⇒ In x-ray diffraction (XRD), there is no isotopic incoherent scattering, but x-ray scattering lengths are *q*-dependent, *i.e.* there is a form factor.

PDF-analysis of local structure
Henry E. Fischer

Basic Concepts
r & t scales, coherence
constructive interference
diffraction formalism
structural correlations
total scattering vs Bragg

aPDF-analysis
S(q) and g(r)
PSFs and PPDFs
correlated vibrations
D-W and TDS
q-space vs *r*-space
$u(r)$ from $g(r)$
aPDF review

aPDF examples
carbon
$\mathrm{BaTi}_{1-x}\mathrm{Zr}_x\mathrm{O}_3$
UO_2
NDIS examples

mPDF-analysis
formalism
generaliities
modeling/simulation

mPDF examples
$\mathrm{SrGd}_2\mathrm{O}_4$
$\mathrm{Gd}_2\mathrm{O}_3$
$\mathrm{Gd}_2\mathrm{Ir}_2\mathrm{O}_7$
EuPtGe
mPDF conclusions

Case of a monoatomic sample (cont'd)

The *static structure factor* (dimensionless) is then given by

$$S(\mathbf{q}) = \int_{-\infty}^{+\infty} d\omega \;\; S(\mathbf{q},\omega) \;\; = \frac{1}{N}\left\langle \sum_{i,j}^{N} e^{i\mathbf{q}\cdot\mathbf{r}_{ij}} \right\rangle$$

and reduces to a real-valued sum of sinc() functions:

$$S(q) = \frac{1}{N}\left\langle \sum_{i,j}^{N} \frac{\sin(qr_{ij})}{(qr_{ij})} \right\rangle$$

in the case of conical Debye-Scherrer diffraction from an isotropic sample (*e.g.* powder, polycrystal, liquid, glass) for which

$$q = |\mathbf{q}| = (4\pi/\lambda)\;\sin(\theta)$$

and 2θ is the diffraction angle with respect to to the incident beam. Finally, for an incident flux Φ and a detector cell of solid angle $d\Omega$, the measured intensity (counts/s) from an isotropic sample is given by

$$I(q) = \Phi\;\frac{d\sigma}{d\Omega}(q)\;d\Omega$$

which, notably, is a function of *q only*.

S(*q*) for a glass or liquid (isotropic, monoatomic)

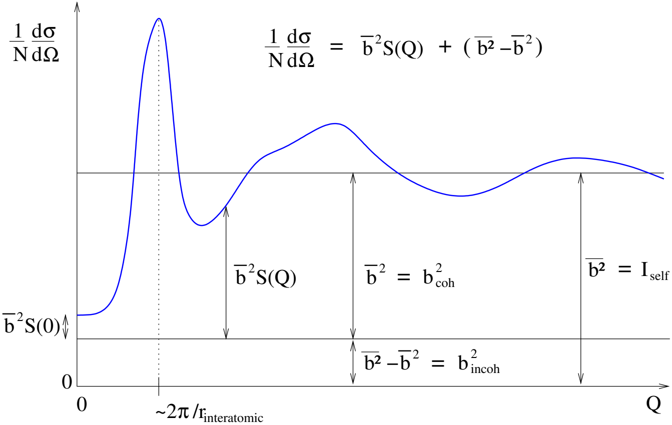

Lack of long-range order, *i.e.* a short structural correlation length ζ_{str}, leads to broad peaks in the diffraction pattern for a glass/liquid, as opposed to sharp (resolution-limited) peaks for a crystalline powder of much greater ζ_{str}. In addition, $\tau_{coh} \sim 1$ fs $\ll \tau_{str} \sim 1$ ps = time scale of atomic displacement in a liquid, providing a "snapshot" of its structure.

Real-space functions (monoatomic case), PDF(r)

Fourier transform gives the *pair-distribution function $g(r)$* which is proportional to the probability of finding an atom at a distance r from an average atom taken as the origin:

$$g(r)-1=\frac{1}{2\pi^2 r\rho_o}\int_0^\infty q\,[S(q)-1]\sin(qr)\,dq$$

in addition to the density function $D(r)$ (also called $G(r)$) used for "PDF-analysis":

$$\mathrm{PDF}(r)=G(r)=D(r)=4\pi r\rho_o\,[g(r)-1]$$

$$=\frac{2}{\pi}\int_0^\infty q\,[S(q)-1]\sin(qr)\,dq$$

as well as the radial distribution function:

$$\mathrm{RDF}(r)=4\pi r^2\rho_o\,g(r)$$

whose integration across peaks yields atomic coordination numbers.

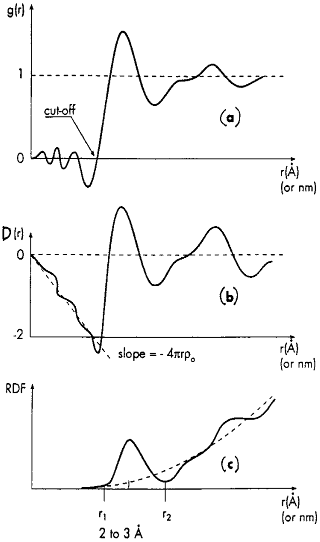

Case of a polyatomic sample (several Z)

In a polyatomic system, the chemical affinities of n different atomic species Z_α necessarily leads to a correlation at atomic sites $\mathbf{r}_i$ between the structural environment and the average scattering length $\overline{b}_\alpha$. This correlation prevents a proper definition of a dimensionless $S(q)$, but the scattered intensity can still be expressed as the sum of a distinct term (the interference function $F(q)$) and a total self-scattering term:

$$\frac{1}{N}\left[\frac{d\sigma}{d\Omega}(q)\right] = \sum_{\alpha,\beta}^{n} c_\alpha c_\beta \overline{b}_\alpha \overline{b}_\beta^* \left[S_{\alpha\beta}(q) - 1\right] + \sum_{\alpha}^{n} c_\alpha \overline{b^2}_\alpha \,,$$

where c_α is the fraction or concentration of atomic species Z_α, and the *partial* structure factor (PSF) $S_{\alpha\beta}(q)$ is the Fourier transform of the *partial* pair-distribution function (PPDF) $g_{\alpha\beta}(r)$, which is in turn proportional to the probability of finding an atom of type Z_β at a distance r from an atom of type Z_α taken as the origin:

$$g_{\alpha\beta}(r) - 1 = \frac{1}{2\pi^2 r \rho_o} \int_0^\infty q \left[S_{\alpha\beta}(q) - 1\right] \sin(qr)\, dq \,.$$

Atomic distributions in glass/liquid versus crystal

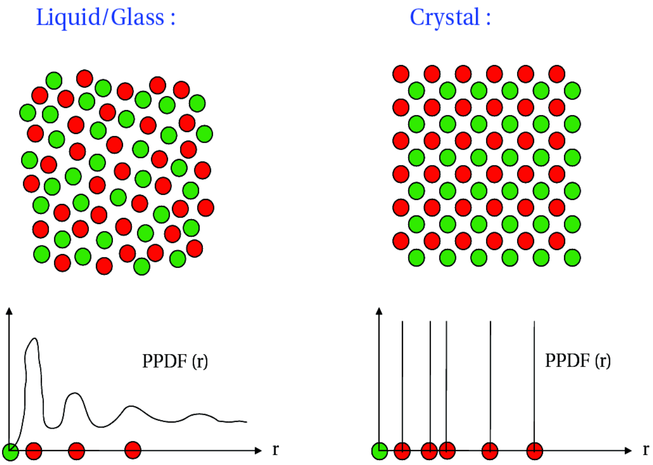

These *partial* PDFs or PPDFs (*e.g.* from NDIS) represent an ensemble average of quasi-instantaneous spatial correlations between red and green atoms: more specifically $g_{GR}(r)$ is proportional to the average probability of finding a Red atom at a distance r from a Green atom.

Vibration modes seen by Rietveld vs PDF-analysis

Whereas Rietveld refinement gives time-averaged distances between atomic pairs, PDF-analysis of total scattering sees an ensemble average of quasi-instantaneous atomic positions and relative distances:

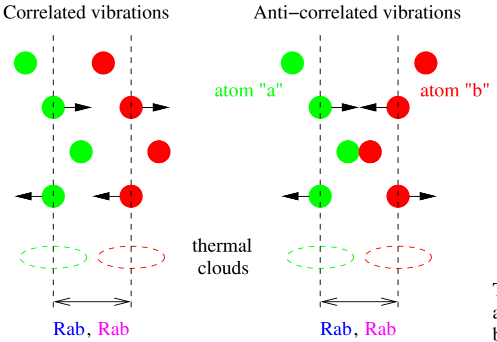

Rietveld−refined Rab = PDF−analysed Rab
for both correlated and anti−correlated vibrations, but Rietveld's time−averaged thermal clouds cannot distinguish between the two cases.
PDF(r) will however show a broader peak for the a−b atomic pair in the anti−correlated case.

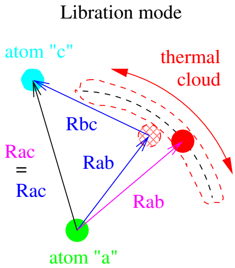

The time−averaged position of atom b is the barycenter of its banana−shaped thermal cloud, which is closer to atom a than any instantaneous position:

Rab (too short) < Rab (correct)

PDF(r) will show a sharp peak for the a−b and a−c atomic pairs but a very broad peak for b−c.

Effect of correlated atomic vibrations at low-r

At short interatomic distances the peaks in $\mathrm{PDF}(r)$ are sharper and taller (conserving area $\propto$ coordination number) as compared to the neutron coherence volume's $\mathrm{FWHM} \sim 60$ Å for the D4c diffractometer:

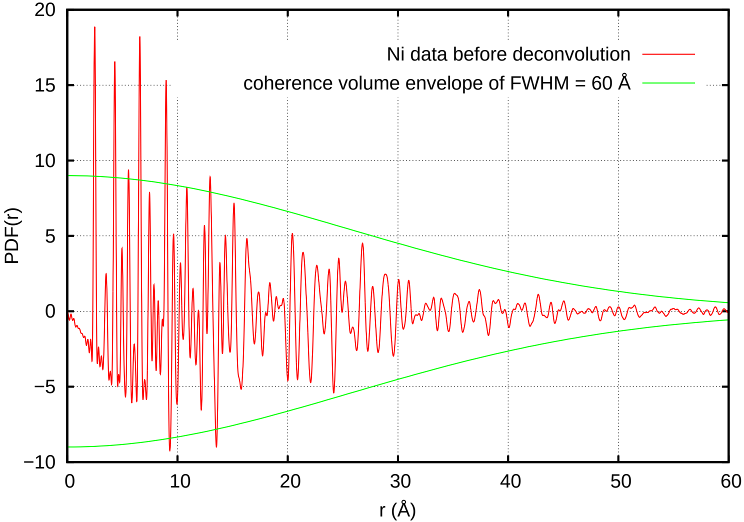

Debye-Waller factor and Thermal Diffuse Scattering

Increased amplitudes of atomic vibration **u** at higher T lead to broader time-averaged “thermal clouds” of atomic positions that reduce Bragg peak intensities via the Debye-Waller factor: $\exp[-\langle(\mathbf{Q}_{hkl}\cdot\mathbf{u})^2\rangle]$:

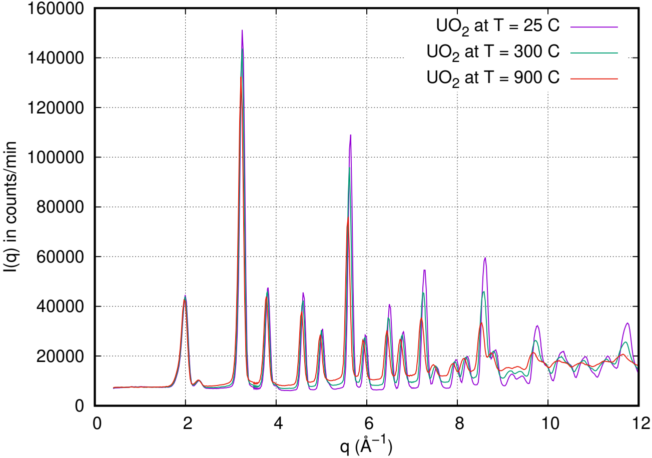

The lost intensity becomes Thermal Diffuse Scattering (TDS) at the base of the Bragg peaks.

The Debye-Waller factor in *q*-space

NB: For a cubic crystal: $\langle(\mathbf{Q}_{hkl}\cdot\mathbf{u})^2\rangle = 2W = Q^2\langle u^2\rangle/3$.

The D-W factor is therefore a *q*-space modulation that reduces the amplitude of a Bragg peak *without affecting its width,* thus reducing its integrated intensity. The Bragg peak positions naturally shift to lower *q* as the lattice expands at higher temperature.

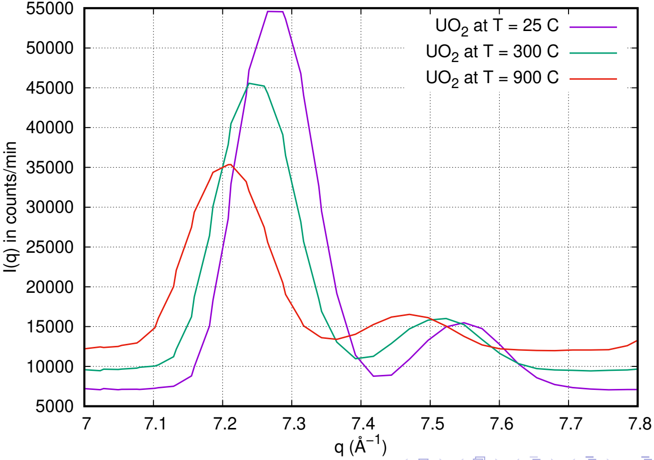

The Debye-Waller factor in *q*-space

The D-W factor's (Gaussian-like) modulation of intensity in *q*-space, *i.e.* reduction of Bragg peak intensity especially at higher *T*, is particularly noticeable when diffraction data are taken up to high-*q*:

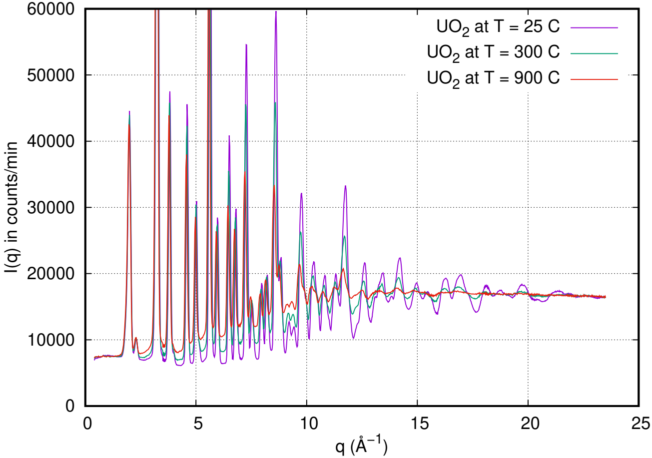

Such reduction in signal at "high harmonics" in *q* should, after Fourier transform, lead to broader features in *r*-space.

The Debye-Waller factor in *r*-space

The convolution theorem states that a modulation in *q*-space leads to a convolution in *r*-space (and vice-versa), such that the the D-W factor broadens the peaks in $\mathrm{PDF}(r)$ according to the vibration amplitudes of the corresponding atomic pairs, *while preserving the peak areas* which are proportional to (generally constant) coordination number:

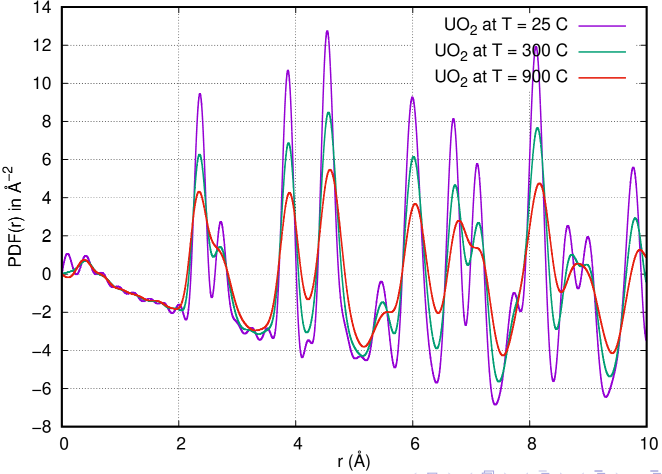

q-space versus r-space representations of data

Diffraction data at high q_{max} show decreasing Bragg-peak intensities due to the Debye-Waller effect (thermal averaging of atomic positions), from static disorder, and also because of limited q-space resolution:

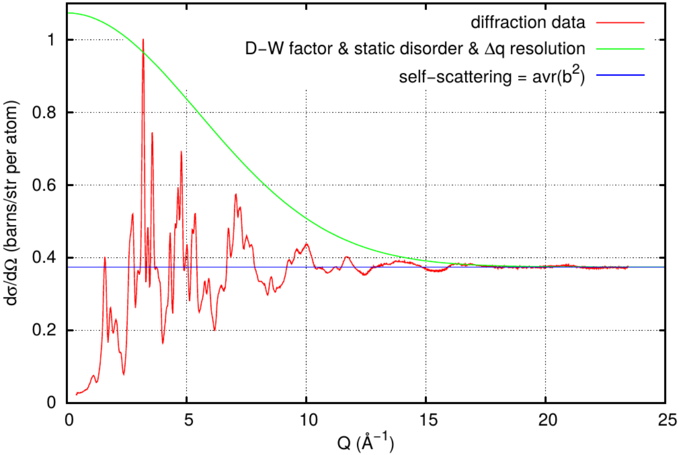

The diffraction intensity ultimately converges to the self-scattering limit $I_{\mathrm{self}} = \overline{b^2}$ when q_{max} is high enough.

q-space versus *r*-space representations of data

The diffuse scattering “underneath” the Bragg peaks, subtracted away as “background” by Rietveld refinement, contains information about dynamic disorder (*e.g.* Thermal Diffuse Scattering = TDS) and static disorder (*e.g.* lattice-constant fluctuations $\Delta a/a$). The Bragg peak widths are generally limited by the instrumental resolution Δq:

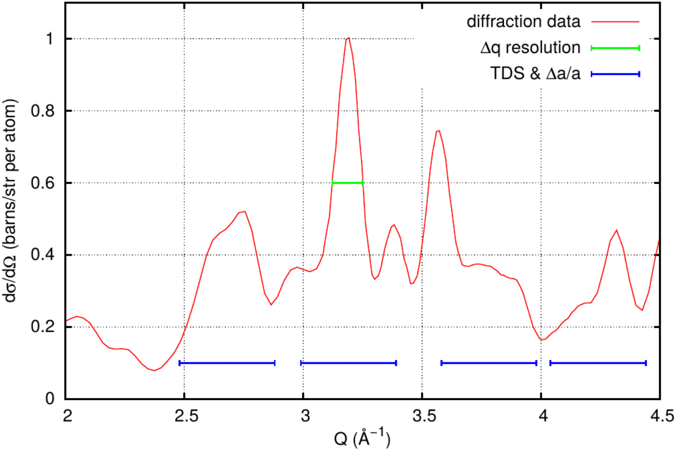

q-space versus *r*-space representations of data

Fourier transform gives the total Pair-Distribution Function $\mathrm{PDF}(r)$ for an average atom at the origin ⇒ peaks at all interatomic distances:

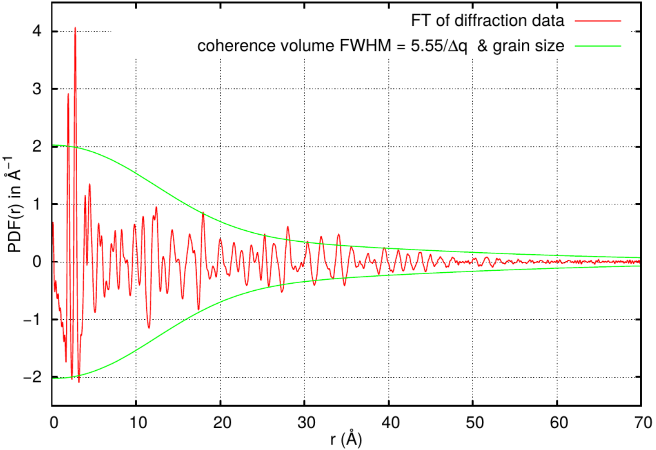

The *r*-range is limited by the crystallographic domain size (*i.e.* the range of structural correlation) and by the coherence volume of the neutron that depends on the *q*-space resolution Δq.

q-space versus *r*-space representations of data

The low-*r* slope of a properly normalized $\mathrm{PDF}(r)$ gives ρ_0, the peak areas are proportional to coordination number for atomic pairs, whose peak widths scale with their dynamic+static disorder plus the *r*-space resolution function $\Delta r(r) = \mathrm{sinc}(q_{\max} r) = \sin(q_{\max} r)/(q_{\max} r)$ that also leads to non-physical FT ripples or “wiggles” at low-*r*:

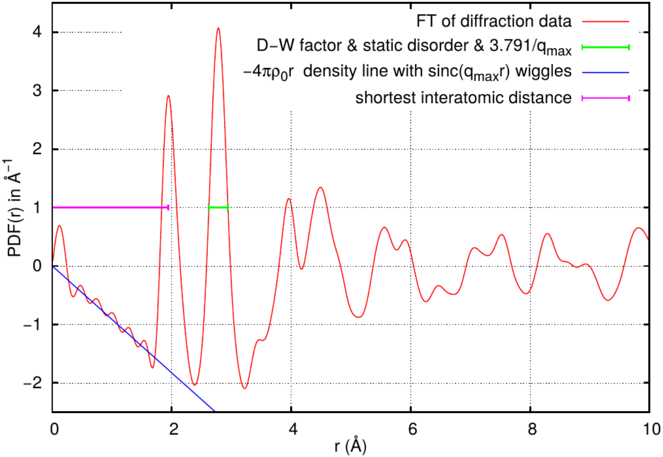

Disorder can mean more information, not less

For an ergodic system like a monoatomic fluid at temperature T, and in the low-density limit, a *classical* mean-field theory relates $g(r)$, obtainable from diffraction, to the interatomic pair potential:

$$u(r) = -k_B T \ln[g(r)]\,,$$

from which follows the interatomic force $\mathbf{F}(r) = -\overrightarrow{\mathrm{grad}}[u(r)]$, and thereby v_{sound}, etc. For realistic densities, an iterative procedure leads to an effective pair potential $u_{\mathrm{eff}}(r)$ (*e.g.* EPSR analysis).

In effect, the $t = 0$ distribution of interatomic distances given by $g(r)$ for a liquid or glass “probes” the shape of $u(r)$, since energetically unfavorable distances will be more rare than favorable ones. By contrast, diffraction measurements on a crystalline sample cannot give such detailed information about $u(r)$ without recourse to modelling.

Note that the above expression also implies that $g(r)$, the structure measured via diffraction, is *independent of atomic mass* in a classical picture. Any observed differences in structure, *e.g.* between the $(d\sigma/d\Omega)(\mathbf{q})$ of H_2O vs D_2O as measured by x-ray diffraction, are necessarily due to QM effects.

Atomic PDF-analysis: FT of a powder diffractogram

Disordered, nano-structured or reduced-dimensional crystals often lack sufficient long-range order to produce sharp diffraction peaks. It is then advantageous to sacrifice q-space resolution by using short wavelengths to provide a high $q_{\max}$ and thus better r-space resolution $\Delta r = 3.79/q_{\max}$ after Fourier Transform (FT) of the diffraction pattern taken as $d\sigma/d\Omega - \mathrm{self\_scattering}$.

The resulting Pair-Distribution Function PDF(r) is the distribution of relative interatomic distances with respect to an average atom at the origin (*i.e.* an ensemble of quasi-instantaneous local structures $\neq$ the time+space averaged structure from Rietveld).

Instrumental q-space resolution Δq determines the neutron's coherence volume seen as an envelope that modulates and limits the spatial extent of the PDF(r) via $r_{\max} = (5.55/2)/\Delta q$.

NB: The PDF(r) is not the output of structural refinement, and is therefore a *model-independent* result that can of course then be used as input for structural modelling/simulation in r-space, thus concluding the technique of (atomic) "**PDF-analysis**".

Atomic PDF(r) examples

Local structure of various forms of carbon

Q-space:

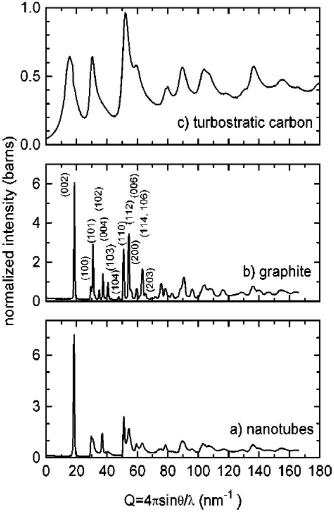

R-space:

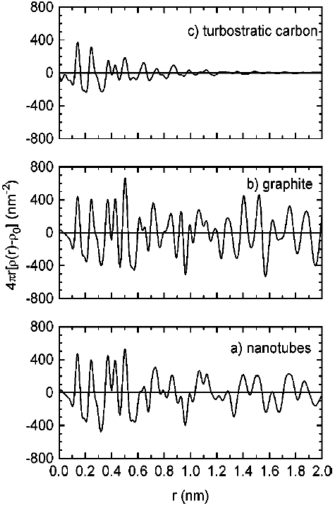

A. Burian, et al, *Phys. Rev. B* **59** *(1999) 1665–8.*

Cation size effect in $BaTi_{1-x}Zr_xO_3$ relaxors

Bragg peak refinement shows that $BaTi_{1-x}Zr_xO_3$'s crystallographic structure is ABO_3 cubic perovskite for $x = 0$ and over the relaxor ferroelectric range ($0.25 \leq x \leq 0.5$) which includes the null-alloy composition $x = 0.32$. As charge disorder is minimized by the isovalent substitution Ti^{4+}/Zr^{4+}, it can be hypothesized that the long-range ferroelectric order is impeded by local structural distortions resulting from the large difference in the two cationic radii.

$\Rightarrow$ PDF-analysis using $\lambda = 0.5$ Å gave unambiguous evidence that the Ti and Zr atoms do not occupy equivalent octahedral sites as expected from the crystallographic structure, but rather the Ti atoms are displaced along [111].

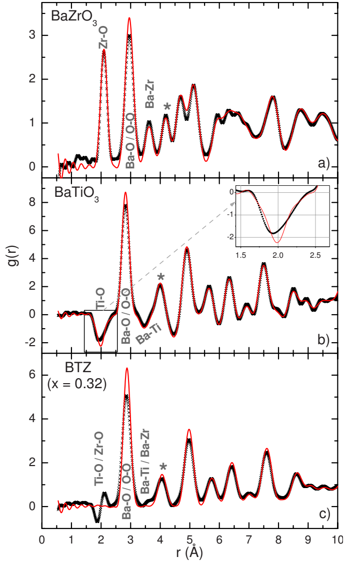

C. Laulhé, et al, *Phys. Rev. B* **79** *(2009) 064104.*

Local, time-correlated atomic displacements in UO$_2$

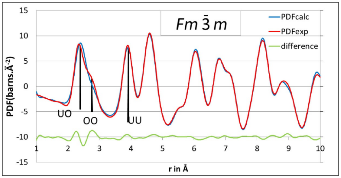

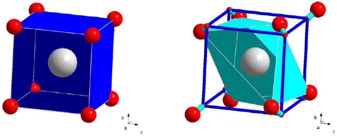

Figure 1. Uranium polyhedron coordination in *Fm*3̄*m* (left) and *Pa*3̄ (right). Uranium and oxygen atoms are colored gray and red, respectively.

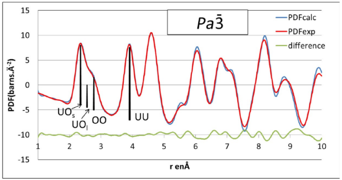

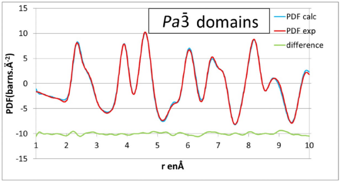

PDF-analysis of UO$_2$ at 1273 K reveals an asymmetric first-neighbor U-O peak, expected from anharmonic atomic vibrations, that could be explained by (highly damped) *dynamically* correlated O-atom thermal displacements of local Pa-3 symmetry, *i.e.* lower than the space+time averaged Fm-3m symmetry.

L. Desgranges, et al, *Inorg. Chem.* **56** *(2017) 321.*

L. Desgranges, et al, *J. Phys. Condens. Matter* **35** *(2023) 10LT01.*

Neutron Diffraction with Isotope Substitution (NDIS)

The technique of Neutron Diffraction with Isotopic Substitution (NDIS) is a powerful method for determining PSFs. It takes advantage of the distribution in isotopes of one or several elements Z_α in the sample, in order to modify $\bar{b}_\alpha$. One must therefore prepare several samples that are chemically and structurally "identical" but of different isotopic distribution. Each sample will give a different diffractogramme $d\sigma/d\Omega$.

Subtraction of two such diffractogrammes cancels the contributions of certain atomic pairs in the sample, yielding thereby a "first-difference function" whose Fourier transform contains information on the local environment of the isotopically substituted species only.

For a binary system ($n = 2$) there are 3 partial structure factors: S_{11}, S_{22} et $S_{12} = S_{21}$, and therefore 3 NDIS samples are sufficient for a complete PSF determination, *e.g.* using a 3×3 matrix of scattering lengths and concentrations that links the 3 NDIS total diffraction patterns to the 3 PSFs.

For more information on NDIS techniques, see *e.g.* the review paper: *H.E. Fischer*, et al*, Rep. Prog. Phys.* **69** *(2006) 233–299.*

NDIS example: First-difference function

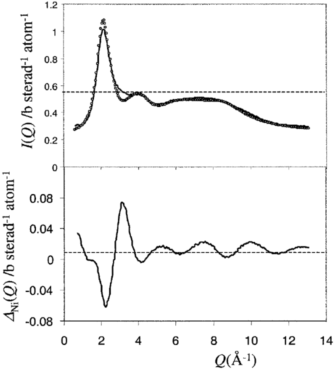

Total structure factors (top) for D_2O solutions of $^{62}NiCl_2$ versus $^{nat}NiCl_2$. Subtraction (bottom) gives a “first-difference” $\Delta_{Ni}(q)$ retaining only those partial structure factors for atomic pairs including a Ni atom.

(D.H. Powell, JDN11 proceedings)

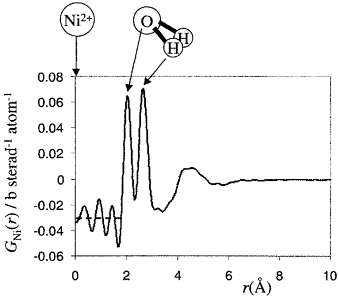

Fourier transformation leads to a first-difference pair-distribution function $G_{Ni}(r)$ showing the distribution of atoms with respect to a Ni atom at the origin. Assuming identical atomic environments for ^{62}Ni and ^{nat}Ni, NDIS thus reveals this local structure.

NDIS example: Complete PSF determination

molten Ag_2Se (ILL) :

< *Barnes et al., J. Phys. Condens. Matter 9 (1997) 6195* >

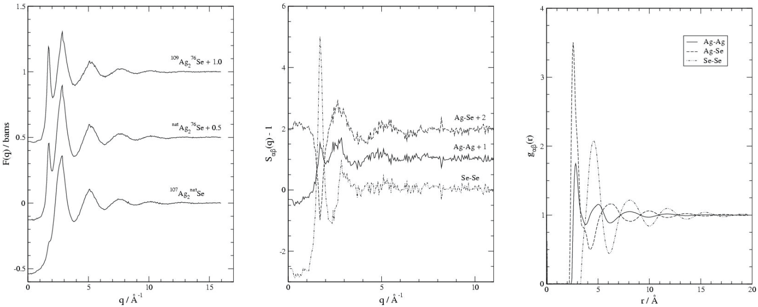

3 $d\sigma/d\Omega$ 3 partial S(q)'s 3 partial g(r)'s

The anti-phase correlations in the partial $g_{\alpha\beta}(r)$ extend to large r, indicating a relatively strong charge ordering consistent with maintaining electroneutrality in this ionic binary liquid, whose local structure is found to resemble that of the high-temperature crystal phase.

Scattering length contrast from XRD vs NRD

The difference in scattering lengths between x-rays and neutrons leads to different diffraction intensities for a given sample, which can also be exploited to obtain partial structure factor information.

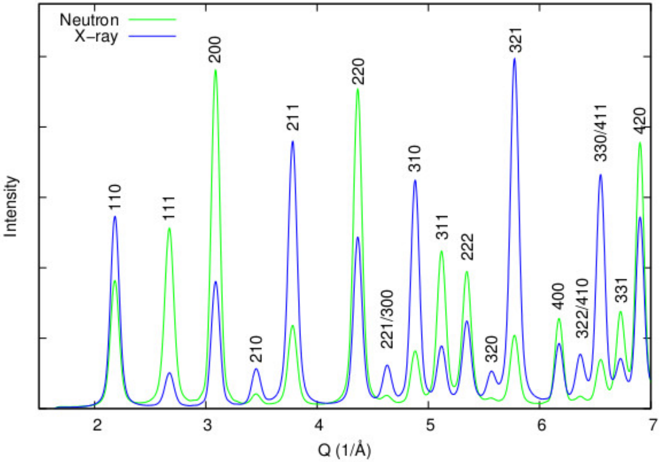

Anomalous X-ray Diffraction (AXD)

The atomic scattering length for x-ray diffraction is independent of isotope but dependent on q and on the incident energy E_o :

$$b_\mathrm{X}(q,E_\mathrm{o}) = r_e\, f(q,E_\mathrm{o}) = r_e\left[Z\, f_\mathrm{falloff}(q) + f'(E_\mathrm{o}) + if''(E_\mathrm{o})\right]$$

where $r_e = 2.818$ fm is the classical radius of the electron, and $f_\mathrm{falloff}(q)$ is the modulation of the atomic form factor $f(q,E_\mathrm{o})$. The technique of Anomalous X-ray Diffraction (AXD) varies E_o (*e.g.* at a synchrotron) and thereby adjusts the real (f', left) and imaginary (f'', right) parts of the scattering length, especially near an absorption edge (here for Se):

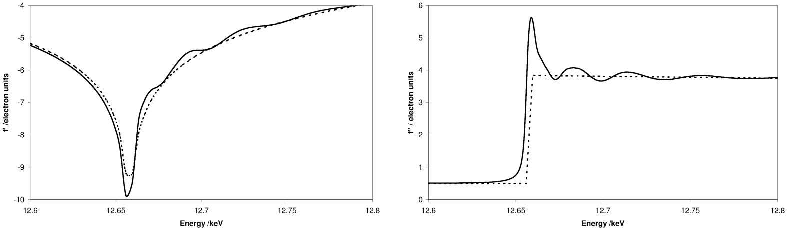

AXD is therefore analogous to NDIS.

Magnetic PDF-analysis

Generalizing to magnetic total scattering

Recall the total (nuclear) differential scattering cross-section per atom:

$$\frac{1}{N}\frac{d\sigma}{d\Omega} = \overline{b}^2\,[S(Q)-1] + \overline{b^2}$$

which comprises a “distinct” term (interference between different atoms) and a “self” term $\overline{b^2}$ (self-interference from individual atoms). As first derived by Blech and Averbach (1964), the total *magnetic* differential scattering cross-section per atom for a system of N identical spins is:

$$\left.\frac{1}{N}\frac{d\sigma}{d\Omega}\right|_{\mathrm{m}} = p^2\mu^2 f^2(Q)$$

$$\cdot\left\{\frac{2}{3}+\frac{1}{N}\sum_{i\neq j}\left[\hat{A}_{ij}\frac{\sin(Qr_{ij})}{Qr_{ij}}+\hat{B}_{ij}\left(\frac{\sin(Qr_{ij})}{(Qr_{ij})^3}-\frac{\cos(Qr_{ij})}{(Qr_{ij})^2}\right)\right]\right\},$$

where μ is the atomic magnetic moment in units of Bohr magnetons μ_{B}, $p=\gamma_n r_e/2 = 2.696$ fm, $f(Q)$ is the magnetic form factor with $f(0)=1$, and $\hat{A}_{ij}$ and $\hat{B}_{ij}$ are spin-spin orientational correlation functions for spin components respectively perpendicular (*i.e.* transverse) or parallel (*i.e.* longitudinal/collinear) to the interspin vector $\mathbf{r}_{ij}=\mathbf{r}_j-\mathbf{r}_i$.

Generalizing to magnetic total scattering

Now define the neutron magnetic scattering length (unpolarized case):

$$b_{\mathrm{m}}(Q) \overset{\mathrm{def}}{=} \sqrt{\frac{2}{3}}\, p\, \mu\, f(Q)$$

The magnetic self-scattering per atom of the magnetic species is then:

$$\left.\frac{d\sigma}{d\Omega}\right|_{\mathrm{m,self}} = b_{\mathrm{m}}^2(Q) = \frac{2}{3} p^2 \mu^2 f^2(Q)$$

and corresponds to the magnetic diffraction intensity per spin in the absence of orientational correlations between neighboring spins. Such a sample with zero spin-spin correlations is simply in the paramagnetic state. Since we are interested precisely in the correlations between magnetic spins, we subtract the magnetic self-scattering from the total magnetic differential scattering cross-section to obtain:

$$I_{\mathrm{m}}(Q) \overset{\mathrm{def}}{=} \frac{1}{N} \left.\frac{d\sigma}{d\Omega}\right|_{\mathrm{m}} - b_{\mathrm{m}}^2(Q)$$

$$= p^2 \mu^2 f^2(Q) \cdot \frac{1}{N} \sum_{i \neq j} \left[\hat{A}_{ij} \frac{\sin(Qr_{ij})}{Qr_{ij}} + \hat{B}_{ij} \left(\frac{\sin(Qr_{ij})}{(Qr_{ij})^3} - \frac{\cos(Qr_{ij})}{(Qr_{ij})^2} \right) \right].$$

The magnetic Pair-Distribution Function mPDF(r)

Recall that the atomic PDF(r) is obtained by Fourier transform of $S(Q)-1$, namely the diffraction intensity $d\sigma/d\Omega$ per atom after subtraction of the self-scattering $\overline{b^2}$ and division by $\overline{b}^2$:

$$\mathrm{PDF}(r) \;=\; \frac{2}{\pi}\int_0^\infty Q\,[S(Q)-1]\,\sin(Qr)\,dQ \;=\; \frac{1}{N}\sum_{i\neq j}^{N}\frac{1}{r}\delta(r-r_{ij})\,.$$

Likewise the normalized self-scattering-subtracted magnetic diffraction intensity $I_{\mathrm{m}}(Q)$ can also be analytically Fourier transformed (first done by B.A. Frandsen, *et al* in 2014) to produce the *model-independent* magnetic Pair-Distribution Function or mPDF(r):

$$\mathrm{mPDF}(r) \overset{\mathrm{def}}{=} \frac{2}{\pi}\int_0^\infty Q\,\frac{I_{\mathrm{m}}(Q)}{\frac{2}{3}p^2\mu^2}\,\sin(Qr)\,dQ$$

$$\approx \frac{3}{2}\cdot\frac{1}{N}\sum_{i\neq j}\left[\frac{\hat{A}_{ij}}{r}\tilde{\delta}(r-r_{ij}) + \hat{B}_{ij}\frac{r}{r_{ij}^3}[1-\tilde{\Theta}(r-r_{ij})]\right],$$

that represents both static and dynamic local spin-spin correlations, where the delta-function $\tilde{\delta}(r-r_{ij})$ and the Heaviside step function $\tilde{\Theta}(r-r_{ij})$ have been broadened by $\mathrm{FWHM_R} \approx 4\ln(4)/\mathrm{FWHM}_{f^2(Q)}$ since we chose for experimental reasons not to divide $I_{\mathrm{m}}(Q)$ by $f^2(Q)$.

Generalities about magnetic PDF-analysis

For non-polarized neutron diffraction from 1 pair of F or AF magnetic spins, $f(r) = \mathrm{mPDF}(r)$ clearly indicates whether the spins' orientation is transverse (showing a strong peak) or longitudinal/collinear (showing a strong slope at low-r) with respect to the interspin vector $\mathbf{r}_{ij} = \mathbf{r}_j - \mathbf{r}_i$.

ferromagnetic:

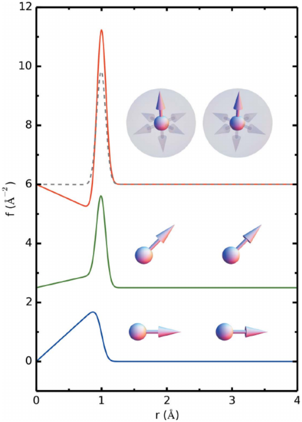

anti-ferromagnetic:

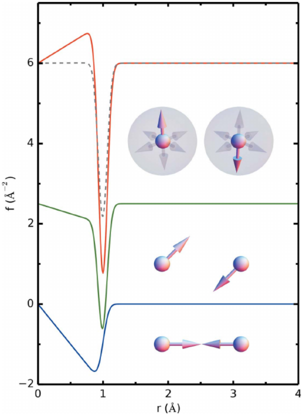

B.A. Frandsen, et al, *Acta. Cryst. A* **70** *(2014) 3–12.*

Generalities about magnetic PDF-analysis (cont'd)

In 1D and 3D systems, transverse versus collinear magnetic structures for F/AF can generally be distinguished respectively by positive/negative peaks versus positive/negative low-*r* slopes in the mPDF(*r*), except in the case of rotational invariance imposed by cubic lattice symmetry.

AF 1-D chain of spins:

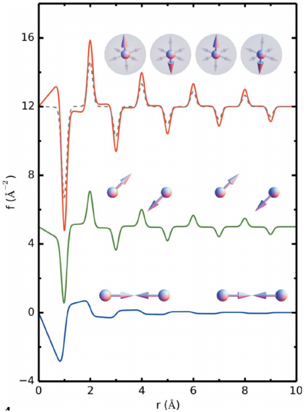

AF 3-D cubic structure:

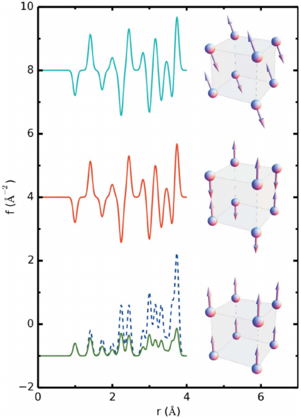

B.A. Frandsen, et al, *Acta. Cryst. A* **70** *(2014) 3–12.*

Modeling techniques for Magnetic PDF-analysis:

Small box modeling (*e.g.* the diffpy.mpdf module for DiffPy-CMI) :

- R-space based *refinement* of spin orientations and perhaps other parameters to fit the measured mPDF(r) – similar to PDFgui, MolPDF.
- Small number of spins, perhaps only one magnetic unit cell.
- Qmax and Qmin are inputed to simulate experimental conditions.
- Additional parameters to dampen and/or broaden the mPDF, simulating the effects of thermal motion and instrumental resolution.

⇒ Runs fast, fits directly the mPDF(r), but susceptible to mixing instrumention effects with structural features.

Large box modeling (*e.g.* Spinvert, RMCprofile) :

- Q-space based *Reverse Monte Carlo* simulation of spin orientations to fit the measured magnetic diffuse scattering $I_{\mathrm{m}}(Q)$.
- Large number (thousands) of spins, corresponding to the dimensions of the neutron coherence volume.
- The fit to $I_{\mathrm{m}}(Q)$ is FT-ed to produce the simulated mPDF(r).

⇒ Accurately treats instrumention effects, can smooth out noisy data, permits sampling of spin-spin correlation functions, but runs more slowly and can be susceptible to maximum-entropy effects and local minima.

Magnetic PDF(r) examples

Magnetic frustration in $SrGd_2O_4$ (*Pnma*, No. 62)

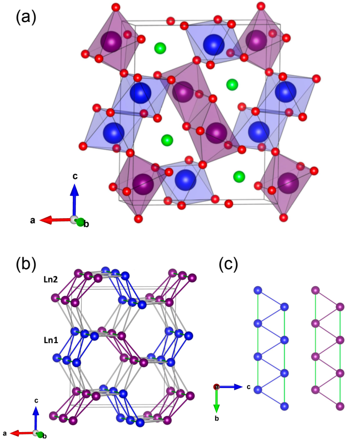

(a) The orthorhombic unit cell of the $SrGd_2O_4$ structure. The magnetic Gd ions occupy two distinct 4*c* Wyckoff sites having octahedral O-coordination and forming around Sr atoms distorted hexagons. (b) The *distorted honeycomb structure* of the magnetic ions manifests along the *b*-axis two types of *zig-zag ladders* (shown in (c)) containing triangles that induce a large degree of *geometrical frustration* due to the NN anti-ferromagnetic exchange.

The two slightly different crystallographic environments of the Gd ions at two distinct 4*c* Wyckoff sites $(x, \frac{1}{4}, z)$ leads to different magnetic ordering in the case of strong CEF effects. Rietveld results (D20@ILL) show that $SrGd_2O_4$ exhibits *longitudinal F* order along each 1D chain but AF correlations between the two chains of a given zig-zag ladder.

Diffraction data for $SrGd_2O_4$ (D4c@ILL, $\lambda = 0.5$ Å)

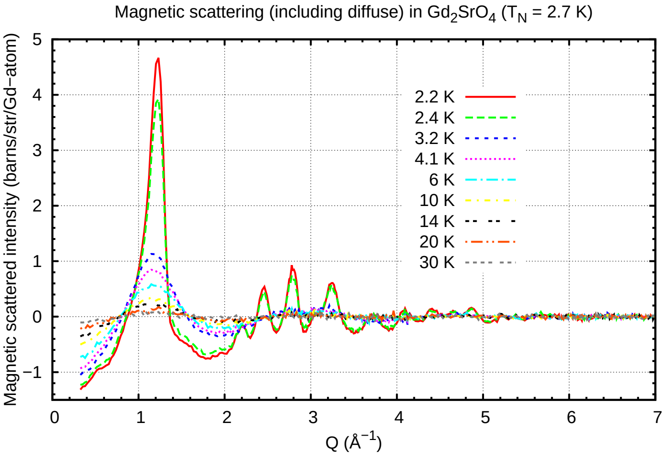

After subtraction of a 50 K "paramagnetic baseline", representing the *Q*-dependent magnetic self-scattering, and normalization via vanadium to an absolute diffraction intensity scale as $d\sigma/d\Omega$.

mPDF(r) data for $SrGd_2O_4$ (D4c@ILL $\lambda = 0.5$ Å)

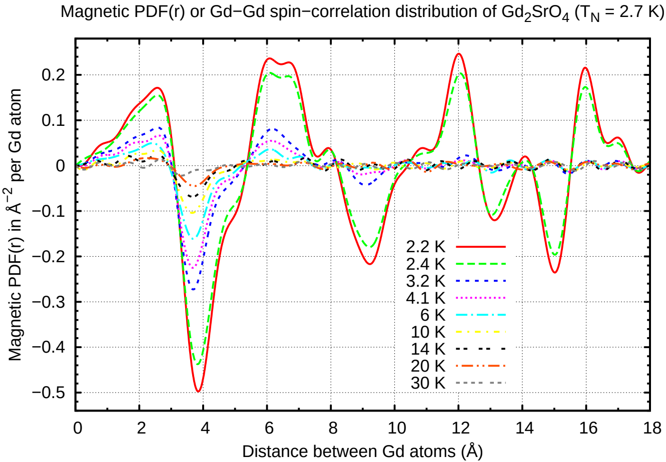

Fourier transform for $Q_{\max} = 7$ $Å^{-1}$ after dividing by the magnetic self-scattering $\frac{2}{3}p^2\mu^2$ (*i.e.* sans form factor squared $f^2(Q)$).

N. Qureshi, et al, *Phys. Rev. B* **106** *224426 (2022).*

Reverse Monte Carlo simulations using SPINVERT

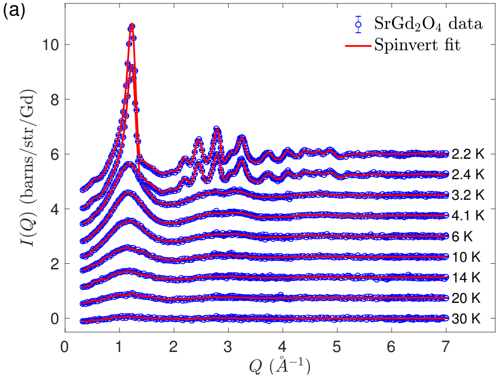

RMC simulations using SPINVERT* fit well the intensity-normalized, 50K-subtracted magnetic diffraction data in *Q*-space ($T_N = 2.7$ K).

Ising spins $\parallel$ *b* are used in a simulation box of 9 x 27 x 9 unit cells that corresponds to the $\sim$ 60 Å spherical neutron coherence volume, and thus to the *Q*-space resolution, of the D4c neutron diffractometer.

J.A.M. Paddison*, et al, *J. Phys.: Condens. Matter* **25 *(2013) 454220.*

r-dependence of the spin-spin correlations

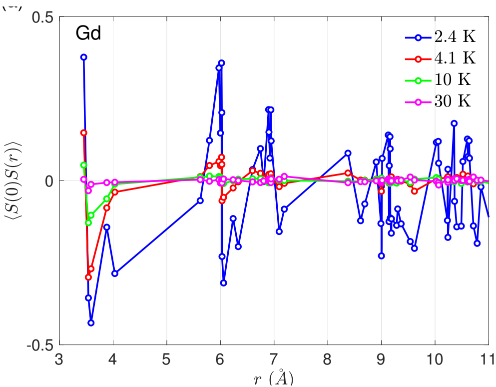

The simple dot-product spin-spin correlation function $\langle \mathbf{S}(0) \cdot \mathbf{S}(r) \rangle$, obtained from the RMC fits, gives the ensemble-averaged alignment between two identifiable spins at a given instant, as separated by the interspin distance r, independent of the direction of the interspin vector $\mathbf{r}_{ij} = \mathbf{r}_j - \mathbf{r}_i$. Clearly observable well above T_N are some short-range *dynamic* spin-spin correlations. Strong correlations at large r indicate long-range *static* correlations (*i.e.* magnetic order) that set in below T_N.

T-dependence of the spin-spin correlations

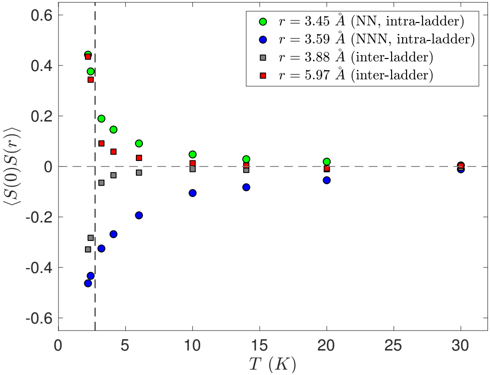

$\langle \mathbf{S}(0)\cdot\mathbf{S}(r)\rangle$ can be obtained from the RMC fits for selected intra-chain, inter-chain (*i.e.* intra-ladder) & inter-ladder distances as a function of T. Strong *intra*-ladder correlations (circles) are observed far above T_N (vertical dashed line). *Inter*-ladder correlations (squares) become important only a few K above T_N. All spin-spin correlations are increasingly dynamic as $T > T_N$, and static as $T < T_N$ (dashed line).

mPDF(*r*) derived analytically and from RMC fits

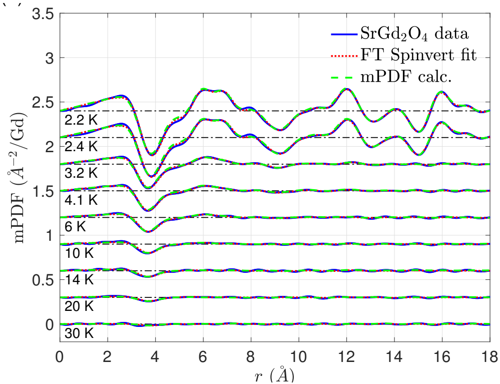

The analytical calculations of the mPDF(*r*) make use of the spin configurations generated by Spinvert, from which are calculated the $\hat{A}_{ij}$ and $\hat{B}_{ij}$ spin-spin orientational correlation functions. The strong positive low-*r* slope confirms the longitudinal F-correlations along 1D chains. The broad negative peak shows the AF correlations between both inter-chain ($r \sim 3.6$ Å) and inter-ladder ($r \sim 3.9$ Å) spins. The positive ~ 6 Å peak indicates ferro NNN-correlations within a hexagon.

D4c and Spinvert results for Gd_2O_3 (monoclinic)

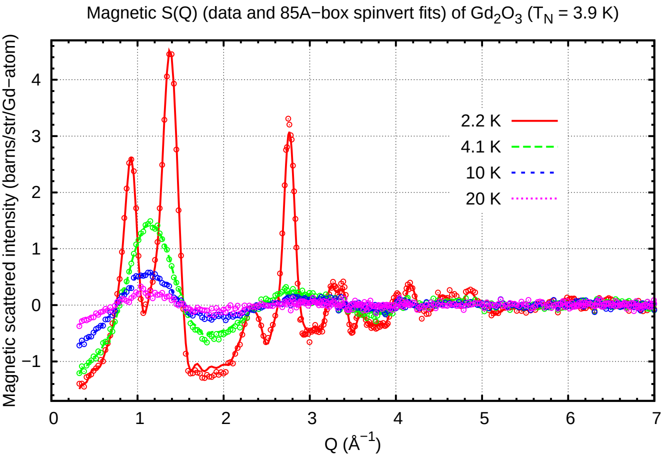

Some quick measurements of magnetic diffraction intensity for the “impurity phase” Gd_2O_3 produced some intriguing results. (Here shown after subtraction of a 50 K “paramagnetic baseline”).

Possible metastable spin configurations above T_N?

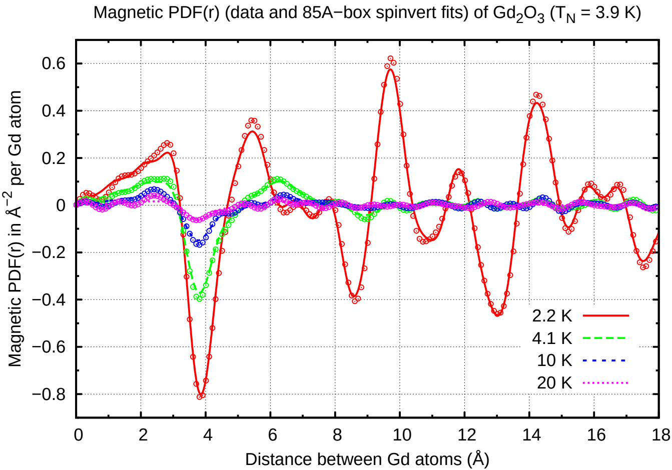

The PDF(r) from the 3D-constrained Spinvert RMC fits in Q-space reproduce the anomalous features at $r = 6$ Å and $r = 9$ Å for $T = 4.1$ K (green curve), corresponding to inter-spin distances that do not show significant correlations in the ordered magnetic structure below T_N.

Unexpected AF correlations in frustrated $Gd_2Ir_2O_7$

Total magnetic scattering in *q*-space (c) and *r*-space (d, 3K-50K):

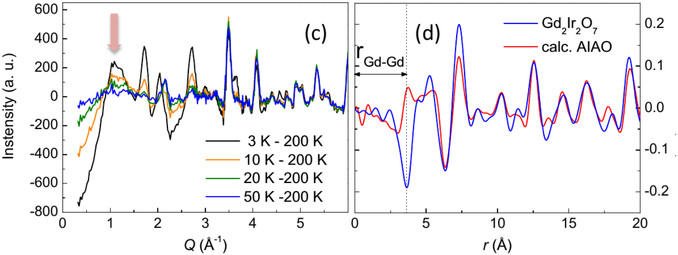

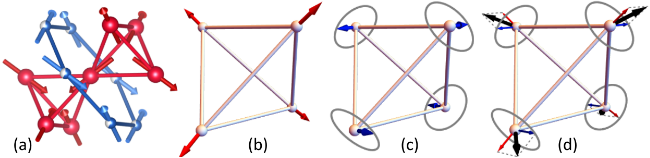

Rietveld: Expected pyrochore AIAO configuration but with a too small ordered Gd moment. **mPDF(r):** Strong AF correlations for NNs ⇒ coexistence of AIAO (a,b) and Palmer-Chalker (c) configurations.

E. Lefrançois, et al, *Phys. Rev. B* **99** *(2019) 060401(R).*

F vs AF correlations in EuPtGe (cubic P2$_1$3, # 198)

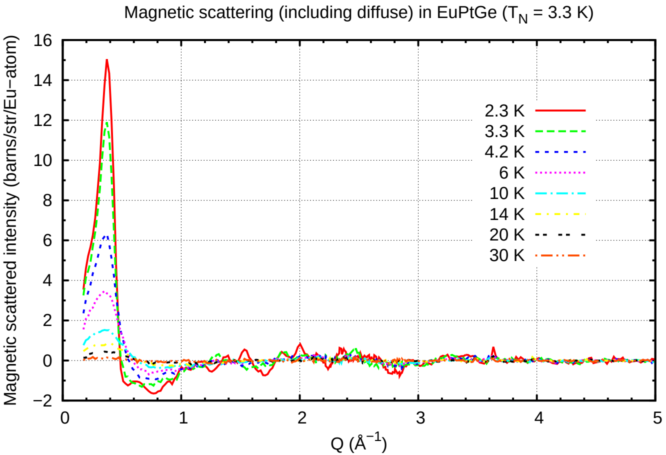

Puzzle : First-order magnetic transition to AF at $T_\mathrm{N} = 3.3$ K but $\Theta_\mathrm{CW} > 0$ from high-*T* susceptibility, hence predominantly F interactions. Specific heat shows spin entropy is recovered only at several times T_N, implying strongly correlated spin fluctuations.

mPDF(r) data for EuPtGe (D4c@ILL, $\lambda = 0.7$ Å)

Magnetic PDF(r) or Eu−Eu spin−correlation distribution of EuPtGe (T_N = 3.3 K)

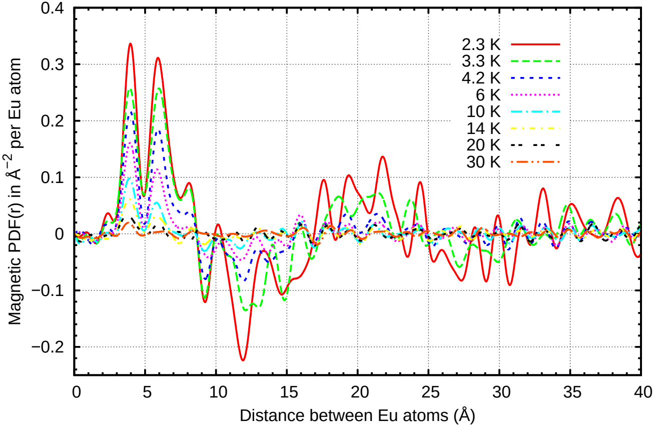

Quick semi-quantitative analysis of the mPDF(*r*) suggests a helical structure ($\sim$ 17 Å period) of Eu^{2+} spins correlated F within a given plane $\perp$ **k**, producing zero net F-ordered moment after *n* planes.

NB: Low-*T* helical phase found in EuPt**Si** from ND/single-crystal: *K. Kaneko*, et al, *J. Phys. Soc. Jpn.* **88** *(2019) 013702.*

Conclusions for magnetic PDF-analysis

Magnetic diffuse total-scattering as measured by neutron diffraction provides quantitative information on short-ranged spin-spin correlations that can be either static (below T_N) or dynamic (above T_N). In contrast, Rietveld refinement provides structural information only as averaged over time and space, very useful for crystallography.

By imposing a physical 3D model of the magnetic system, RMC simulations of magnetic diffuse scattering data allow to derive in a robust way the real-space spin-spin correlation function $\langle \mathbf{S}(0) \cdot \mathbf{S}(r) \rangle$ as a function of interspin distance and temperature, even when the diffraction data are beset by significant statistical noise.

Magnetic PDF-analysis provides a *model-independent* real-space function mPDF(r), obtained directly from the diffraction data, that permits to distinguish longitudinal vs transverse spin-spin correlations, albeit with limited R-space resolution due to the magnetic form factor.

The complementary use of RMC simulations with mPDF-analysis of magnetic diffuse scattering data offers a powerful tool for investigating both static and dynamic spin-spin correlations in disordered magnetic systems, such as those subject to geometrical frustration.

Table of Contents